Selective Etching and Hardness Properties of Quenched SAC305 Solders

Muhamad Zamri Yahaya[1], Nor Azmira Salleh[1], Soorathep Kheawhom[2], Balázs Illés[3] Ahmad Azmin Mohamad[1,*]

[1]School of Materials and Mineral Resources Engineering, Universiti Sains Malaysia, 14300, Nibong Tebal, Penang, Malaysia

[2]Department of Chemical Engineering, Faculty of Engineering, Chulalongkorn University, Bangkok 10330, Thailand

[3]Department of Electronics Technology, Budapest University of Technology and Economics, Budapest, Hungary

*Corresponding e-mail address: aam@usm.my

Tel.: +604 599 6118, Fax: +604 594 1011

Abstract

The morphology of the β-Sn, Ag_3Sn and Cu_6Sn_5 intermetallic compound (IMC) and its' relation to the mechanical properties of the Sn-3.0Ag-0.5Cu (SAC305) solder alloy were investigated in the function of cooling conditions. SAC305 solder joints was cooled down by oven cooling, air cooling, water quenching, and ice quenching after a reflow process. Three different etching methodswere applied in order to be able to investigate the IMC phases.. Specific indentation pattern was used to determine the Vickers microhardness. The reduction of the XRD peak intensities showed the influence of the cooling condition on the forming of the different phases.. The selective etching allowed depth observation on the phases and accurate measurement on the thickness of the Cu_6Sn_5 layer. The water- and ice-quenching resulted in significant size reduction of the rod-like Cu_6Sn_5 and thread-like Ag_3Sn as well as the refinement of the grain structure. This was resulted in the improvement of the mechanical properties, since the highest hardness value of 16.05 Hv was observed in the case of ice-quenched SAC305 solder joints.

Keywords: SAC305; reflow soldering; IMC; Electrochemical Etching; Hardness

1. Introduction

Soft solders are metal alloys which are usually used to join mechanically and connect electrically two or more electrical components of the assemblies. Recently, the Sn-Ag-Cu (SAC) solder family, particularly the Sn-3.0Ag-0.5Cu (SAC305) alloy, is the leading lead-free solder alloy being used in the electronics industries [1]. The intermetallic (IMC) phases within the solder joints mainly determine the properties of SAC305 solder joints. The fine Cu_6Sn_5 and Ag_3Sn phases in the β-Sn matrix can improve the mechanical properties of the SAC305 solder joints [2]. However, there are many factors, such as phase migration [3], thermal aging [4, 5], type of the substrate [6], and solidification rate [7], which can facilitate the formation of larger IMC phases. The larger IMC phases impede lower dislocation movements, which is clearly not advantageous as this will result in more unsatisfactory mechanical performance (such as the reduction on the tensile and hardness properties). Among these aforementioned factors, the solidification rate is the most significant.

The cooling rate affects the morphologies of the Ag_3Sn and Cu_6Sn_5 phases. Lee et al. found that rapid cooling like 63.17 °C s^{-1} resulted in the formation of a very fine Ag_3Sn network and suppresses the formation of Cu_6Sn_5 IMC layer, thereby improving the tensile strength up to 60.8 MPa [8]. Tsao et al. reported that small Ag_3Sn precipitates, obtained by water cooling at 102 K s^{-1}, also increased the hardness of the SAC305 alloy from 12.1 Hv to 13.6 Hv [9]. The previous findings clearly highlighted the strong relationship between IMC microstructure and the cooling conditions. The investigation of the solder joints microstructure usually applies only on 2D cross-sections to study the size and the morphology of the IMC phases. However, different etching technologies can be applied to investigate 3D morphology of the IMC phases. During etching, the inter-dendritic elements are removed by an electrochemical reaction to allow excellent observations of the remaining dendritic core of the IMC phases [10, 11]. Wang et al. used deep etching technique on SAC305 solder joints and found a complex Ag_3Sn

network around large rod-like Cu_6Sn_5 [1]. The removal of the β-Sn matrix achieved by the selective electrochemical etching also revealed the significant differences on the morphologies of the SAC305 prepared by the vapour phase soldering and CO_2 laser soldering techniques [12]. As the IMC layer plays an important role on the reliability of the solder joint, it is important to perform the detail observation and analysis on these layers obtained by the different cooling conditions. Mechanical evaluation like hardness tests is also essential to further correlate the morphological observations with the mechanical properties of the SAC305 [13]. This information is crucial to understand the influence of the cooling conditions on the reliability of the solder joint upon application/operation.

In this work, SAC305 solder joints were prepared with different cooling conditions. Cyclic voltammetry (CV) was used to set a suitable etching potential. Electrochemical etching was then conducted on the SAC305 solder joints by means of chronoamperometry (CA). Evaluations on the phase, morphology, and hardness were subsequently conducted to investigate the effects of the cooling conditions.

2. Materials and Methods SAC305 paste of the ALPHA CVP-390 (Alpha Assembly Solutions) was printed onto FR4 substrate (2 cm × 3 cm) by a custom stencil with 5 mm in diameter and 1 mm in thickness. The printed SAC305 were reflowed in a reflow oven (TYR-108C, Modell Technology) in accordance with the programmed reflow profile: preheating (160–180 °C), reflowing (213–247 °C), and cooling (247–40 °C).

Different cooling conditions were applied: normal oven cooling, air cooling (26 °C), water quenching (25 °C) and ice quenching (0 °C). Mechanical cutting by a diamond cutter (MICRACUT, Metcon) was conducted prior to 800, 1200, and 2000 grit silicon carbide grinding and 1.0, 0.5, and 0.03 µm alumina suspensions polishing. Electrical connections were

prepared by single core copper wire for the subsequent cyclic voltammetry (CV) and electrochemical etching.

Preliminary CV measurements were carried out in a conventional airtight three electrode cell contains 1% sulphuric acid (H_2SO_4) electrolyte at 25 °C by a potentiostat (Autolab PGSTAT 101). A saturated calomel electrode (SCE) was used as the reference electrode, carbon rod as the counter electrode, and the SAC305 as the working electrode. CV curves were recorded at a scanning rate of 1 mV s^{-1} by a potentiostat operating software, NOVA 11.1.

The polished samples were etched by 0.1 M ferric chloride ($FeCl_3$) etchant. The samples were immersed in 0.1 M ferric acid for 10 s prior to rinsing with distilled water to remove the remaining etchant, and to prevent over etching. This process was carried out in a fume cupboard at ambient temperature.

The deep etching were based from the Jackson method [14]. The polished samples were initially etched in 20 % HNO_3 solution for 5 h. Upon rinsing with distilled water, subsequent etching process in 20 % HCl solution was conducted for 70 h. The samples were then rinsed with distilled water to remove any remaining etchant from the surface. Both etching processes were carried out in a fume cupboard at ambient temperature.

Selective removal of the β-Sn was obtained by a standard three electrode cell connected to the potentiostat (Autolab PGSTAT 101) in chronoamperometry (CA) mode. The cell consists a saturated calomel electrode (SCE) as a reference electrode, carbon rod as counter electrode, and the SAC305 solder alloy as the working electrode. 80 ml of 1% sulphuric acid

(H_2SO_4) was used as an electrolyte. The etching was conducted at a fixed potential bias of -3.5 V with etching duration of 120 s.

The phase and structural analyses were conducted by X-ray diffraction (XRD, Bruker AXS D8 Advance) with monochromatized Cu Kα radiation (λ = 1.5406 Å) in the range of 10° < 2θ < 90°. The morphology of the etched solder was examined by a Field Emission Scanning Electron Microscope (FESEM, 35VP, Zeiss Supra^{TM}) equipped with energy dispersive X-ray (EDX). The thickness of the IMC layer was determined using the SEM images by the ImageJ software.

The hardness evaluations were conducted by a Vickers microhardness tester (Leco Corporation, LM-248AT) with a maximum load of 10 gf and dwell time of 15 s. 10 indentations were carried out on a specific configuration pattern to ensure an accurate hardness acquisition throughout on the entire SAC305 cross-section **(Figure 1)**.

3. Results and Discussion

3.1 Effect of cooling methods on phases of SAC305 solder alloy

First, the XRD analyses of the different samples were done. In the SAC305 solder joints, the following phases are expected: β-Sn (ICSD-98-009-1748), Ag_3Sn (ICSD-98-000-1559) and Cu_6Sn_5 (ICSD-98-010-9332). The oven-cooled samples displayed the highest peak intensities of the Cu_6Sn_5 phase at 46° and of the Ag_3Sn phase at 52.5° (**Figure 2a**). The air-cooled SAC305 showed a lower peak intensity for the Cu_6Sn_5 phase but higher peak intensities for the β-Sn and Ag_3Sn phases than the oven-cooled samples (**Figure 2b**). It was observed that the further increasing the cooling rate with water quenching, the peak intensities of the β-Sn, Ag_3Sn and Cu_6Sn_5 phases significantly reduced (**Figure 2c**), and all of the peaks almost

disappeared in the case of ice-quenched cooling. (**Figure 2d**). Interestingly α-Sn (ICSD-98-009-1898) was also detected in the case of ice-quenching cooling.

The relatively higher peaks of the Ag_3Sn and Cu_6Sn_5 phases in the cases of oven and air-cooling conditions might be attributed to the favourable growth of these phases due to the relatively longer solidification period [15]. The longer cooling time provided by these two conditions allowed the Ag_3Sn and Cu_6Sn_5 phases to coalesce into larger grains, which contribute to the higher peak intensities, as it was observed from the XRD results. In addition, this effect could also explain the significant reduction of peak intensities of the Ag_3Sn and Cu_6Sn_5 phases obtained by the water and ice-quenched cooling conditions. Generally, the faster solidification reduced the growth rate of all phases (both the IMC and β-Sn) which resulted in smaller grains with varying orientations. This made them less detectable during XRD analysis (lower intensities). The appearance of α-Sn phase in the case of ice-quenched cooling was due to the allotropic transition of β-Sn below 13.2 °C [16]. The previous results clearly showed the influence of the cooling condition on the formation of the different phases in the SAC305 solder joints.

3.2 Potential-bias determination and selective electrochemical etching

In the second step, the potential-bias (CV) curves were determined. The CV curves at different cycles show the different reaction peaks for the SAC305 solder alloy, especially along the oxidation region, which is the most significant for the potential selection of the electrochemical etching (**Figure 3**). An oxidation peak appeared at -0.29 V during the anodic period in the first cycle (**Figure 3a**). Then, the second cycle produced two oxidation peaks at -0.49 V and -0.33 V (**Figure 3b**). During the third cycle, both peaks shifted slightly to -0.47 V and -0.35 V (**Figure 3c**).

The single peak of the first cycle is attributed to the dissolution of the β-Sn and IMC phases [17]. It was quite hard to obtain the separate dissolution of the IMC phases during the first cycle since most of the defects from the surface of the cross-sections was removed (mainly due to the grinding and polishing processes). On the second cycle, the appearance of individual peaks for the β-Sn and the IMC phases could be caused by the deposited IMC phases during the first cycle, and the dissolution of the IMC phases during the second cycle from the agitated surface. Considering the stabilization of the method, -0.35 V (from the third cycle) was selected as the suitable potential for the selective removal of β-Sn during the electrochemical etching.

The subsequent electrochemical etching conducted at -0.35 V resulted in a consistent CA plot for all cooling conditions (**Figure 3d**). Generally, the cooling conditions did not have any significant influence on the electrochemical etching process. The initial rapid increase in the current was a good indicator for the instantaneous removal of β-Sn [12]. The higher current in the case of ice-quenched samples was caused by the finer grain structure of the IMC phases, as a result of the fast solidification. Thus, it led to more grain boundaries and more intense dissolution of β-Sn [18].

3.3 Morphological evaluation of the IMC phases attained by different etching methods

Differences in the shape and size of the IMC phases and the IMC layer were observed on the cross-sections after the application of chemical etching technique (**Figure 4**). Generally, the morphologies of the IMC phases were similar for the oven-cooled and air-cooled SAC305 solder joints. The rod-like Cu_6Sn_5 and the thread-like Ag_3Sn were located at the central matrix (**Figure 4a-b**). A scalloped Cu_6Sn_5 IMC layer dominated at the solder-substrate interface. However, the IMC layer in the case of air-cooling was thinner than in the case of oven-cooling. The microstructure changed considerably in the case of rapid cooling methods (water-

quenching and ice-quenching). In the case of water-quenching, the thickness of the scalloped type Cu_6Sn_5 IMC layer reduced significantly and the thread-like Ag_3Sn refined (**Figure 4c**). The ice-quenching refined further the Ag_3Sn phase (**Figure 4d**) and rod-like Cu_6Sn_5 IMC phases were not found in the matrix.

The deep etching method provides more information about the morphological differences of the IMC phases in the case of different cooling conditions (**Figure 5**). This etching method made visible how the thread-like Ag_3Sn network surrounds the Cu_6Sn_5 phases (**Figure 5a-b**). The scallops in the Cu_6Sn_5 IMC layer were less elongated for both cooling conditions in comparison to the micrographs revealed by the chemical etching. Smaller rod-like Cu_6Sn_5 was obtained by the water-quenched SAC305 (**Figure 5c**). A combination of scalloped and planar Cu_6Sn_5 IMC layers also differentiated the morphologies of the water-quenched SAC305. The thread-like Ag_3Sn was significantly refined, with a better distribution throughout the central matrix for the ice quenching condition (**Figure 5d**). The transition from a scalloped to a planar Cu_6Sn_5 IMC layer was also more prominent.

Significant differences in the micrographs were obtained between the chemical and deep etching as a higher volume of β-Sn phase were removed. During solidification, the scallop-type Cu_6Sn_5 IMC layer was found to be the favourable growth of the IMC layer in the SAC305 solder joints. This was caused by the rapid diffusion of Cu into the molten solder [19, 20], and this enabled the Cu_6Sn_5 to grow further towards the central matrix of the SAC305 solder joints. The acquisition of a planar Cu_6Sn_5 IMC layer, especially for the ice-quenched SAC305, was plausible as shorter solidification duration the Cu diffusion. The rapid cooling rate in the case of the water-quenched and ice-quenched solder joints resulted in the decrease of the interfacial energy which caused the refinement of the Ag_3Sn and Cu_6Sn_5 phases and limited the growth of the Cu_6Sn_5 IMC layer [21]. This was mainly due to the almost

instantaneous solidification of the Cu_6Sn_5 and Ag_3Sn precipitates, which inhibited further growth [22].

The IMC phases were most distinguishable after the application of selective electrochemical etching method (**Figure 6**). Micrographs of the oven-cooled SAC305 solder joint showed that it contains large-sized Cu_6Sn_5 rods, which extended from the interface to the centre of the matrix (**Figure 6a**). Height and thickness differences of the scalloped Cu_6Sn_5 IMC layer was clearly observed at the interface. Even a slightly faster cooling rate at air-cooling method reduced the size of the Cu_6Sn_5 rods (**Figure 6b**). However, the Ag_3Sn with high-density refined branch network was still distributed mostly around the Cu_6Sn_5 (**Figure 6c-d**). The distribution of both IMC phases was greatly improved, especially at the central matrix. Such an alteration in the trend continued further in the case of faster cooling provided by the ice-quenching method.

Actual shape of large rod-like Cu_6Sn_5 was attributed only after complete removal of the β-Sn phase. The longer solidification period in the case of oven cooling allowed the Cu_6Sn_5 to grow in the preferred orientation of the rods [15]. In addition, the extension from the Cu_6Sn_5 at the interface indicated further such a favourable growth. Since Cu_6Sn_5 acts as a nucleation sites for the Ag_3Sn precipitates, the dominant position of the Ag_3Sn was near the Cu_6Sn_5 [23]. Faster solidification (in the case of water- and ice-quenching) inhibited the enlargement of the Cu_6Sn_5 and Ag_3Sn precipitates. The previous effects resulted in two main outcomes on the morphology of the SAC305 solder joints, which are the finer and more homogenous grain structure. The small Ag_3Sn precipitates could also suppress the growth of the Cu_6Sn_5 IMC layer [24].

3.6 Thickness of the IMC layer

Unfortunately, the measured IMC thicknesses in the case of the different cooling conditions were moderately influenced by the applied etching method (**Figure 7**). Generally, the IMC thickness decreased with the cooling rate. The average thicknesses of the Cu_6Sn_5 IMC layer, measured on the chemically-etched micrographs, were 4.6 μm (oven-cooling), 3.8 μm (air-cooling), 1.8 μm (water-quenching) and 1.4 μm (ice-quenching). The thickness decreased slightly for all cooling conditions, as measured from the images obtained by the deep etching and selective electrochemical etching method (**Table 1**).

The results clearly indicated that the growth of the Cu_6Sn_5 IMC layer depended highly on the cooling conditions. The IMC layer thickness decrease in the case of higher cooling rates was due to the lower reaction time for the dissolution of the Cu to form Cu_6Sn_5 at the solder-substrate interface [25]. Additionally, the interfacial energy of the growing Cu_6Sn_5 was much lower due to the rapid drop in temperature provided by the water and ice-quenching methods. The differences between the etching methods could be explained with the "efficiency" of each different technique. It was observed that the measured IMC thickness decreased with the increase of the removed amount of β-Sn. A sufficient removal was found in the case of electrochemical etching, which probably enabled the most accurate observation of the scalloped Cu_6Sn_5 IMC layer [10].

3.7 Hardness properties of SAC305 solder joints in the case of different cooling conditions

The different cooling rate resulted in differences in the hardness properties as well (**Figure 8**). It was observed that the hardness increased with the cooling rate. The lowest hardness value of 13.99 HV was measured on the oven-cooled solder joints. The hardness increased slightly to 14.09 HV when air-cooling was applied. The hardness of the water-quenched solder joints increased with 10.36 %, up to 15.44 HV. The highest hardness value of

16.05 HV (14.65 % increase compared to the oven-cooled samples) was measured on the ice-quenched solder joints.

The increase of the hardness value with the increase of the cooling rate was mainly due to the strengthening of the grain boundaries by the IMC phases [21]. The size reduction of the Ag_3Sn and the Cu_6Sn_5 IMC phases, due to the higher cooling rate, resulted in more grain boundaries within the matrix of the solder joints. The grain boundaries act as barriers to dislocation movements during the application of load, thereby providing higher mechanical resistance of the solder joints against deformation [26, 27]. Homogenous distribution of the fine Ag_3Sn and Cu_6Sn_5 IMC phases also hindered the propagation of forces within the matrix [28].

3.8 Mechanism of the IMC formation during different cooling conditions

The growth of the Cu_6Sn_5 IMC layer is mainly determined by the diffusion of Cu atoms (from the substrate) into the molten solder. Different concentration gradients of Cu at the interface encourage the diffusion of Cu [29]. The longer cooling time (at the oven- and air-cooled solder joints) caused prolonged diffusion of the Cu, which induced the growth of the Cu_6Sn_5 IMC layer (**Figure 9a-b**). It resulted in a slightly thicker Cu_6Sn_5 IMC layer in the oven- and air-cooled solder joints due to the extended solidification period. Accordingly, IMC growth was much slower in the case of faster cooling conditions like water- and ice-quenching. Due to the rapid drop in the temperature by the quenching process, the migration of the Cu_6Sn_5 was stopped by the prompt solidification. Therefore, the growth of the Cu_6Sn_5 IMC layer was significantly decreased, resulting in a thinner IMC layer (**Figure 9c-d**). It is also possible that the formation of the Cu_6Sn_5 IMC layer in the quenched solder joints occurred only during the reflow process (since the Cu still diffused into the solder alloy) [30].

The formation of the central matrix in the solder joints can be described with a similar phenomenon. In the oven- and air-cooled solder joints, the IMC phases have got higher interfacial energy due to the slower cooling rate. This was responsible for the formation of the larger-size Cu_6Sn_5 and Ag_3Sn phases. Furthermore, the slow cooling rate also enabled the Cu diffusion from the substrate into the central matrix and supported the formation of Cu_6Sn_5 phases in the central matrix (this explains the occurrence of the long Cu_6Sn_5 rods near the solder/substrate interface) [31].

In the Sn-Ag-Cu system, the faster cooling condition leads to the nucleation of small Ag_3Sn precipitates. Structure and size of the Ag_3Sn phases depends on three factors: the Ag content, the cooling rate, and Cu content [32]. In this case, only the cooling rate changed since the Ag content and Cu content were constant in the SAC305 solder alloy. The faster cooling rate (at water- and ice-quenching) slowed down the growth of the Ag_3Sn phase, thus, a very fine and homogenous Ag_3Sn network formed. During the reflow process, the IMC can form in the melting and solidification stages [33]. At the water- and ice-quenched solder joints, the solidification stage was considerably shortened, which resulted that the IMC formation occurred almost only during the melting stage. This effect also blocked the effective Cu diffusion into the central matrix and prevented the formation of rod-like Cu_6Sn_5 IMC phase, as it was observed in the case of oven- and air-cooled solder joints.

4. Conclusion

The influence of the cooling condition on the formation of IMC phases was investigated by different etching methods. A preliminary electrochemical analysis from the CV measurement determined the potential bias for the electrochemical etching. The current recorded from the CA showed similar current responses in the case of all cooling conditions. The XRD analysis indicated that the peak intensities reduce as the cooling rate increases, which

means the suppression of the grain growth into the preferred orientation due to the rapid solidification. All etching conditions exhibited effective removal of the β-Sn phase. The micrographs prepared by electrochemical etching revealed better observation regarding the shape and texture of the IMC phases than the conventional etching method. Lower grain orientation sensitivity of the electrochemical etching method (unlike chemical etching) significantly improved the micrographs and enabled accurate observation of IMC phases. It was faund that the Ag_3Sn network was significantly refined with the ice-quenching process. Also, the thickness of the Cu_6Sn_5 layer decreased with the increase of the cooling rate. The finer Ag_3Sn network and the thinner Cu_6Sn_5 IMC layer were the results of the reduced solidification time. The ice-quenched solder joints showed the highest hardness values due to the refinement of the Ag_3Sn and Cu_6Sn_5 phases. Consequently, further researches are necessary to determine the optimal cooling rate during reflow soldering process.

Acknowledgements

Muhamad Zamri Yahaya, Nor Azmira Salleh and Ahmad Azmin Mohamad appreciate the financial support provided by the FRGS grant 203.PBahan.6071377 (Ref: FRGS/1/2017/TK05/USM/02/2). Balázs Illés thanks the financial support provided by the National Research, Development and Innovation Office – NKFIH, FK 127970.

References

[1] M. Wang, J. Wang, H. Feng, W. Ke, Corros. Sci., 63 (2012) 20-28.

[2] T. Garami, O. Krammer, J. Mater. Sci-Mater. El., 26 (2015) 8540-8547.

[3] G. Chen, L. Liu, J. Du, V.V. Silberschmidt, Y. Chan, C. Liu, F. Wu, J. Mater. Sci., 51 (2016) 10077-10091.

[4] X. Deng, R. Sidhu, P. Johnson, N. Chawla, Metall. Mater. Trans. A, 36 (2005) 55-64.

[5] J. Wang, H. Nishikawa, Microelectron. Reliab., 54 (2014) 1583-1591.

[6] Y. Liu, F. Sun, H. Zhang, T. Xin, C.A. Yuan, G. Zhang, Microelectron. Reliab., 55 (2015) 1234-1240.

[7] T.-K. Lee, T.R. Bieler, C.-U. Kim, J. Electron. Mater., 45 (2016) 172-181.

[8] H.-T. Lee, K.-C. Huang, J. Electron. Mater., 45 (2016) 182-190.

[9] L. Tsao, S. Cheng, C. Chen, T.-Y. Chen, Mat. Sci. Eng. A-Struct., 658 (2016) 159-166.

[10] T. Hurtony, A. Bonyár, P. Gordon, Microstructure comparison of soldered joints using electrochemical selective etching, in: Mater. Sci. Forum, Trans Tech Publ, 2013, pp. 367-372.

[11] M.Z. Yahaya, A.A. Mohamad, Int. J. Electr. Mater., 5 (2017) 50-55.

[12] T. Hurtony, A. Bonyár, P. Gordon, G. Harsányi, Microelectron. Reliab., 52 (2012) 1138-1142.

[13] S.S.M. Nasir, M.Z. Yahaya, A.M. Erer, B. Illés, A.A. Mohamad, Ceram. Int., (2019).

[14] D. Lewis, S. Allen, M. Notis, A. Scotch, J. Electron. Mater., 31 (2002) 161-167.

[15] D. Mu, H. Yasuda, H. Huang, K. Nogita, J. Alloys Compd., 536 (2012) 38-46.

[16] T.-K. Lee, T.R. Bieler, C.-U. Kim, H. Ma, in: Fundamentals of Lead-Free Solder Interconnect Technology, Springer, 2015, pp. 231-249.

[17] J. Zhang, M. An, L. Chang, Electrochim. Acta, 54 (2009) 2883-2889.

[18] M. Wang, J. Wang, W. Ke, Microelectron. Reliab., 73 (2017) 69-75.

[19] J. Lee, K.C. Chen, K. Subramanian, J. Electron. Mater., 32 (2003) 1240-1248.

[20] R.A. Gagliano, M.E. Fine, J. Electron. Mater., 32 (2003) 1441-1447.

[21] T. Chuang, L. Tsao, C.-H. Chung, S. Chang, Mater. Design, 39 (2012) 475-483.

[22] M. He, Z. Chen, G. Qi, C.C. Wong, S.G. Mhaisalkar, Thin Solid Films, 462 (2004) 363-369.

[23] K. Kim, S. Huh, K. Suganuma, J. Alloys Compd., 352 (2003) 226-236.

[24] X. Liu, M. Huang, Y. Zhao, C.M.L. Wu, L. Wang, J. Alloys Compd., 492 (2010) 433-438.

[25] J.-H. Lee, J.-H. Park, Y.-H. Lee, Y.-S. Kim, D.H. Shin, J. Mater. Res., 16 (2001) 1227-1230.

[26] T.R. Bieler, B. Zhou, L. Blair, A. Zamiri, P. Darbandi, F. Pourboghrat, T.-K. Lee, K.-C. Liu, J. Electron. Mater., 41 (2012) 283-301.

[27] M.Z. Yahaya, A.A. Mohamad, Solder. Surf. Mt. Tech., 29 (2017) 203-224.

[28] M.Z. Yahaya, F.C. Ani, Z. Samsudin, S. Sahin, M.Z. Abdullah, A.A. Mohamad, Mat. Sci. Eng. A-Struct., 669 (2016) 178-186.

[29] W.-Y. Chen, C.-Y. Yu, J.-G. Duh, J. Mater. Sci., 47 (2012) 4012-4018.

[30] X. Hu, T. Xu, X. Jiang, Y. Li, Y. Liu, Z. Min, Appl. Phys. A-Mater., 122 (2016) 278.

[31] J. Gong, C. Liu, P.P. Conway, V.V. Silberschmidt, Scripta Mater., 60 (2009) 333-335.

[32] S.K. Kang, D.-Y. Shih, N. Donald, W. Henderson, T. Gosselin, A. Sarkhel, N.C. Goldsmith, K.J. Puttlitz, W.K. Choi, JOM, 55 (2003) 61-65.

[33] L. Yang, Z. Zhang, J. Electron. Mater., 44 (2015) 590-596.

Figure 1: Schematic diagram of the hardness evaluation by the Vickers microhardness

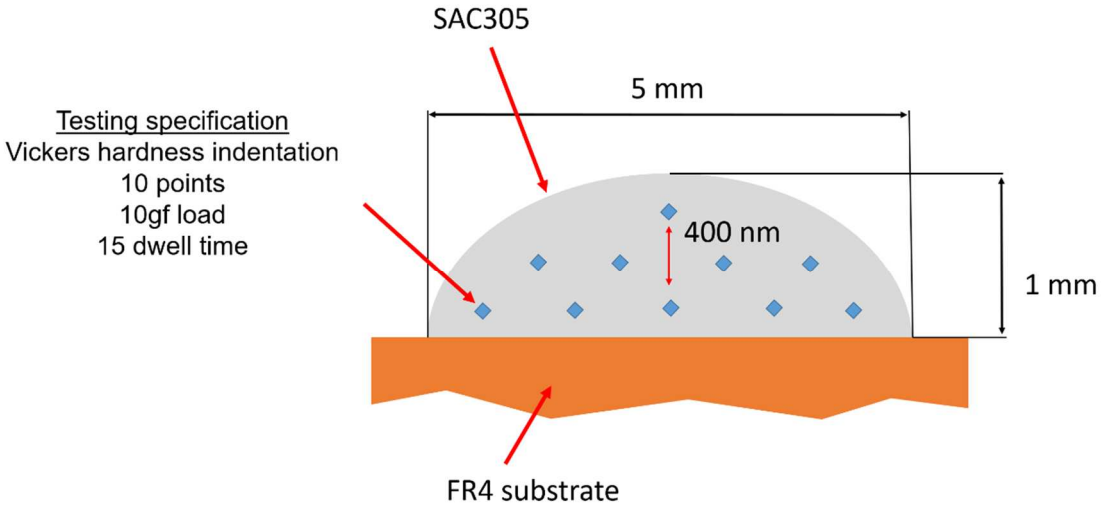

Figure 2: XRD pattern of SAC305 solder joint by different cooling methods (a) oven cooling, (b) air cooling, (c) water quenching and (d) ice quenching

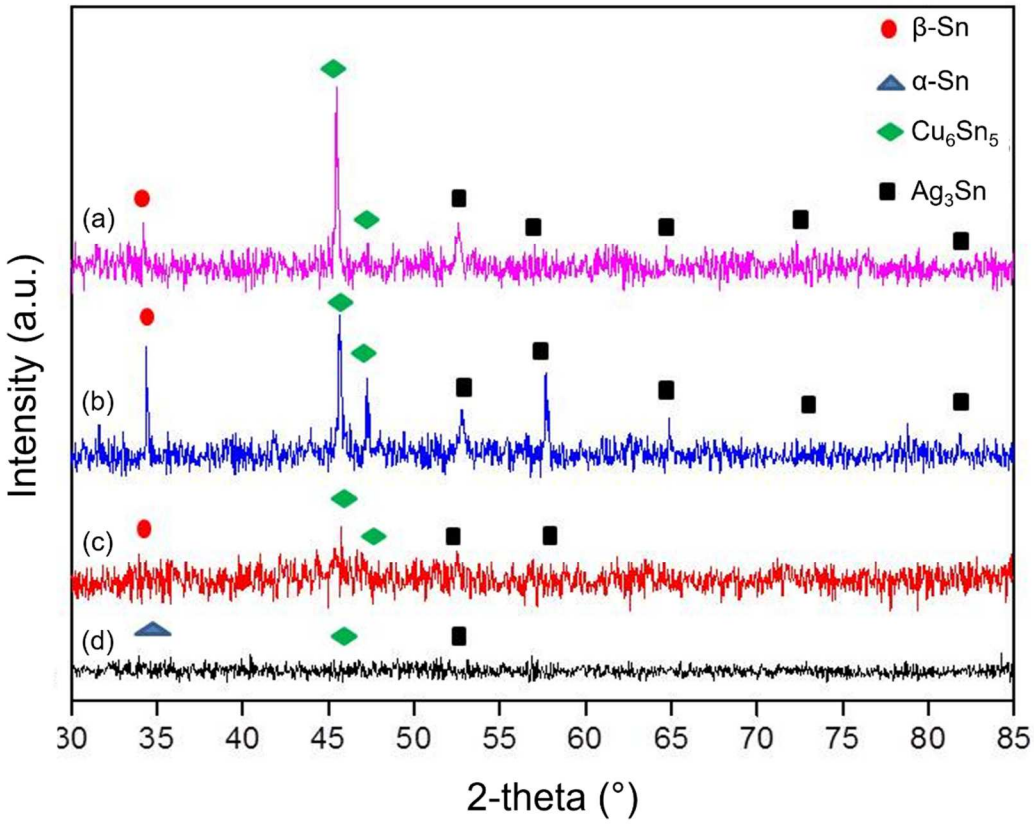

Figure 3: CV curves of SAC305 solder joints for three cycles: (a) first cycle, (b) second cycle, (c) third cycle at scan rate 1 mVs^{-1}, and (d) CA curves of the SAC305 with different cooling condition at 120 s at -350 mVs^{-1}

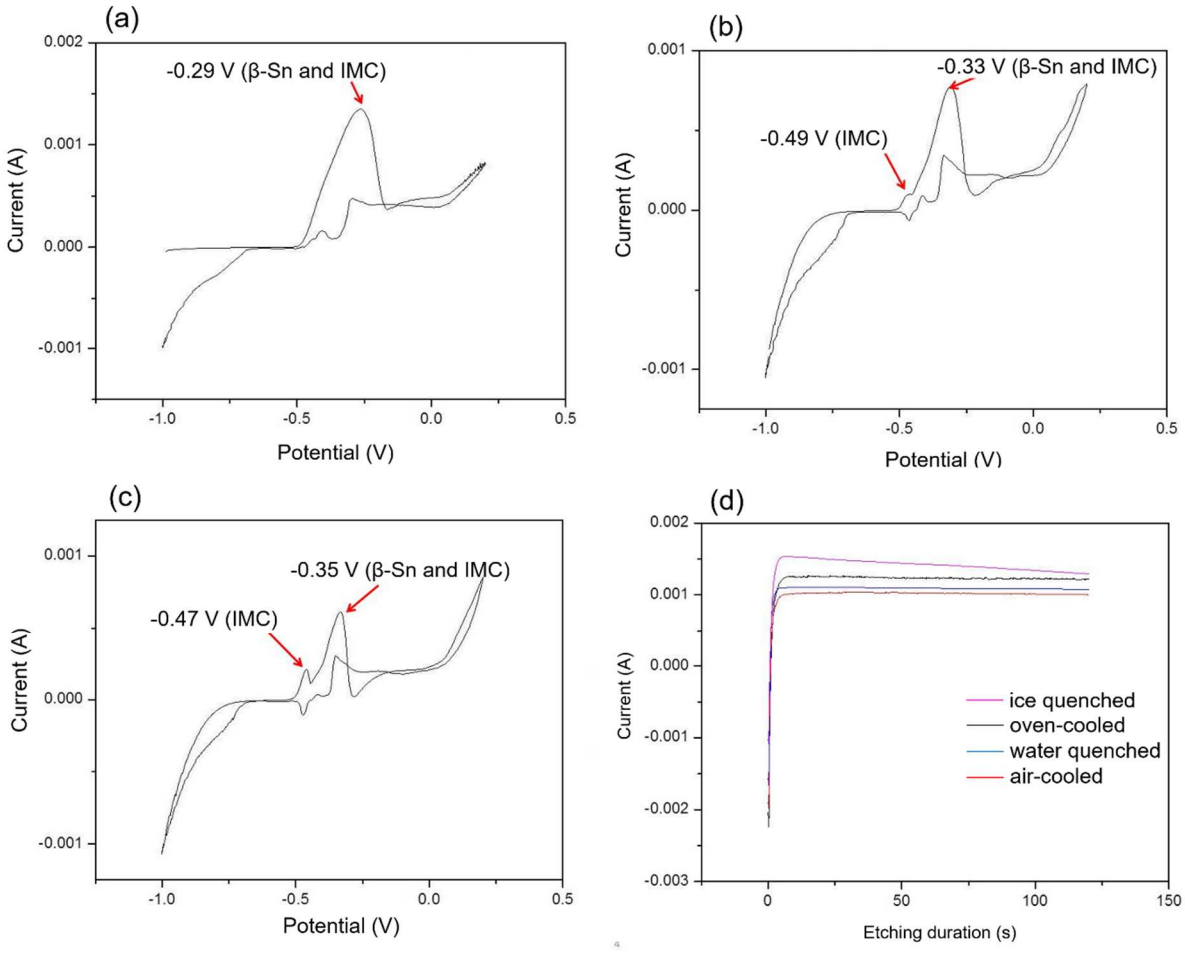

Figure 4: Microstructures of SAC305 solder joints by different cooling methods: (a) oven cooling, (b) air cooling, (c) water quenching, and (d) ice quenching investigated by chemical etching

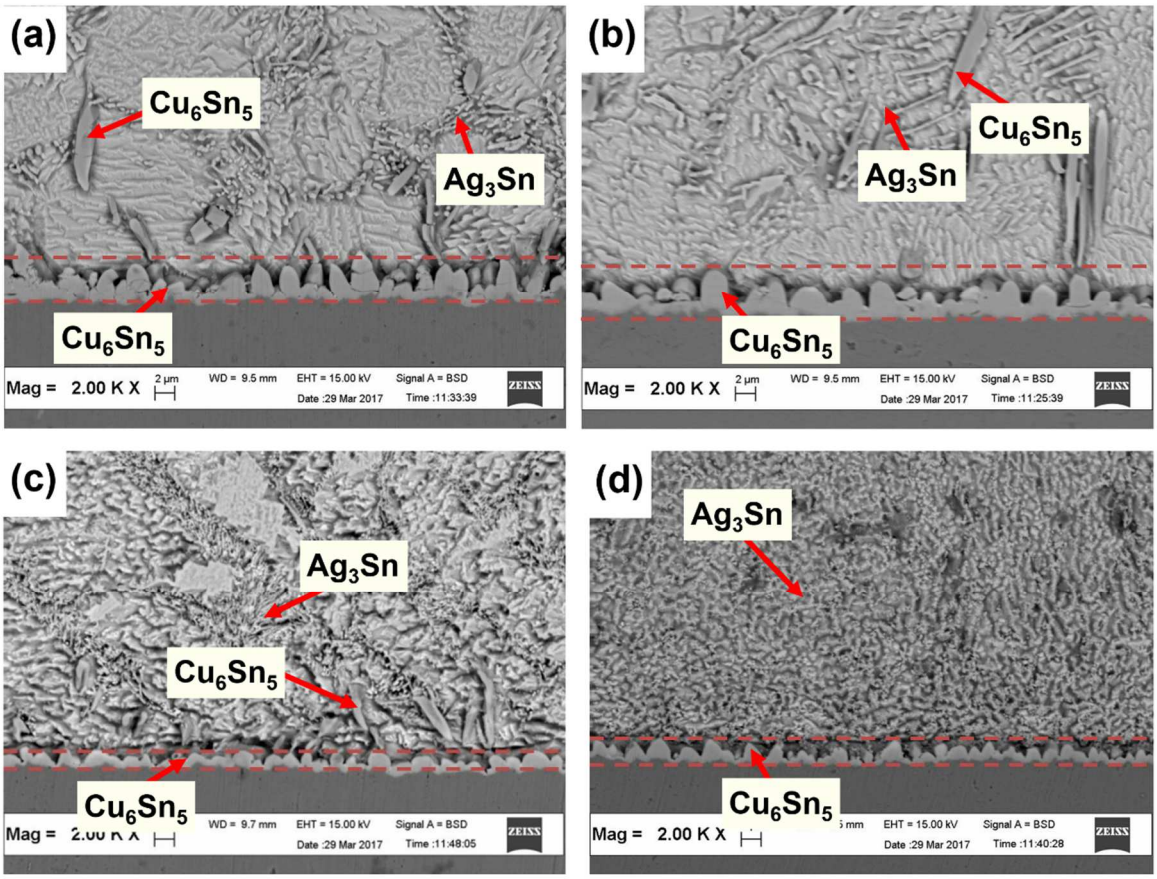

Figure 5: Microstructures of SAC305 solder joints by different cooling methods: (a) oven cooling, (b) air cooling, (c) water quenching, and (d) ice quenching investigated by deep etching

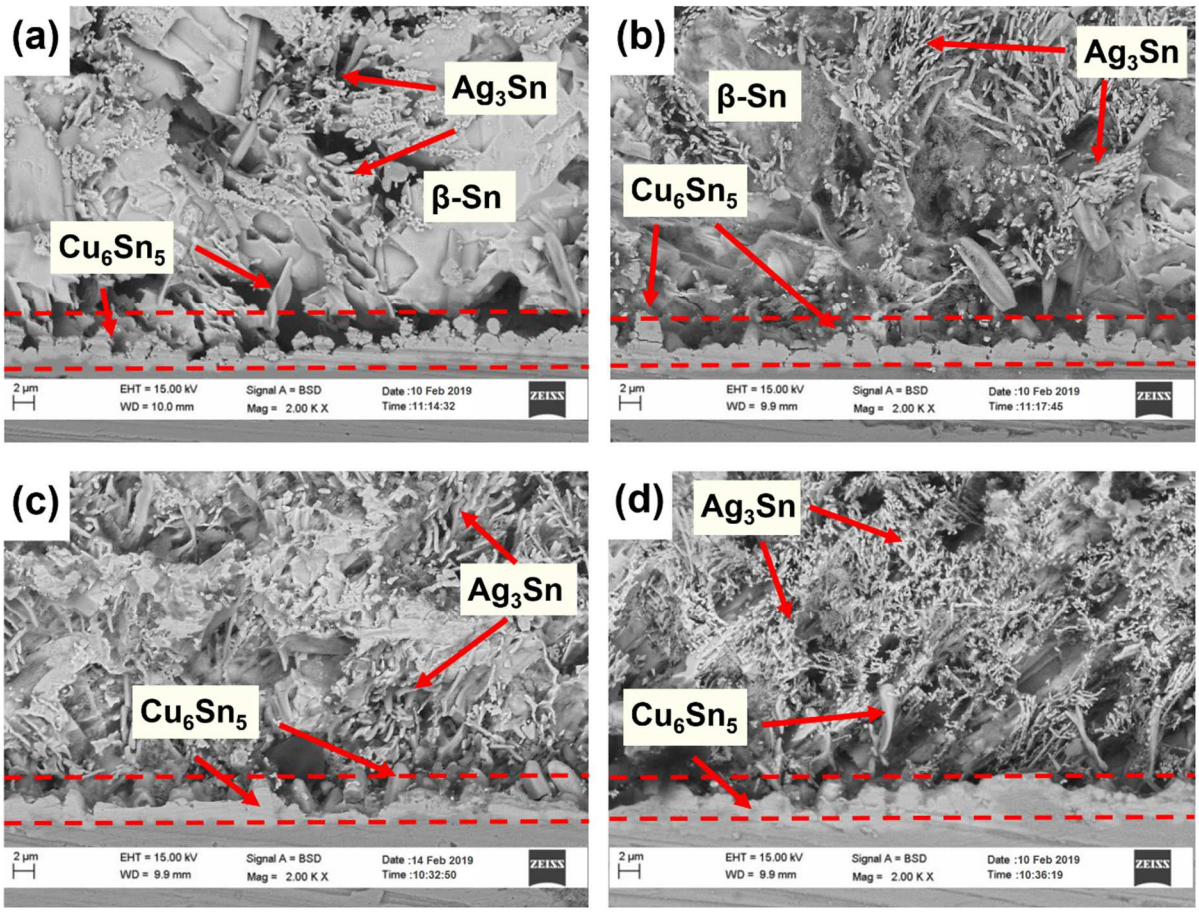

Figure 6: Microstructures of SAC305 solder joints by different cooling methods: (a) oven cooling, (b) air cooling, (c) water quenching, and (d) ice quenching investigated by selective electrochemical etching

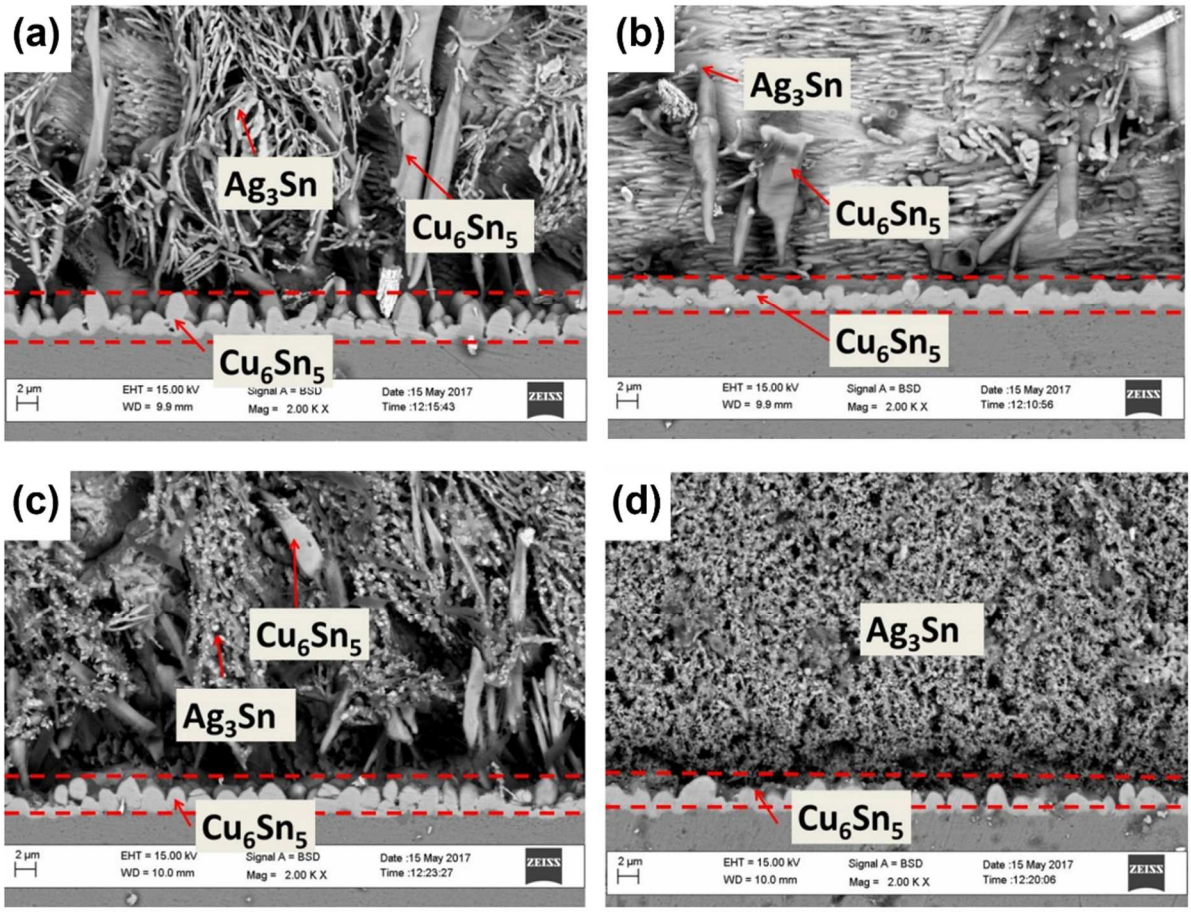

Figure 7: Interfacial Cu_6Sn_5 IMC thickness of SAC305 solders with different cooling methods investigated by chemical, deep and electrochemical etching

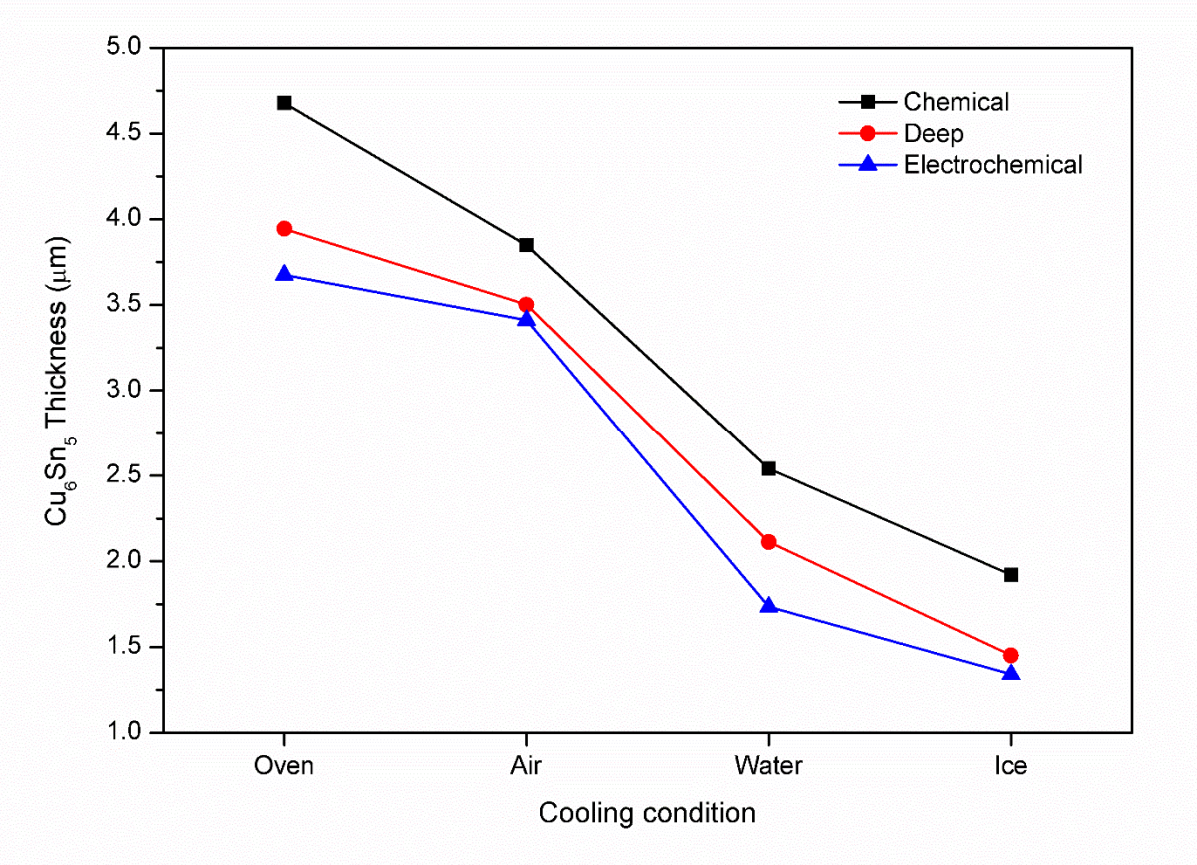

Figure 8: Vickers hardness evaluation on the SAC305 solder joints by different cooling conditions.

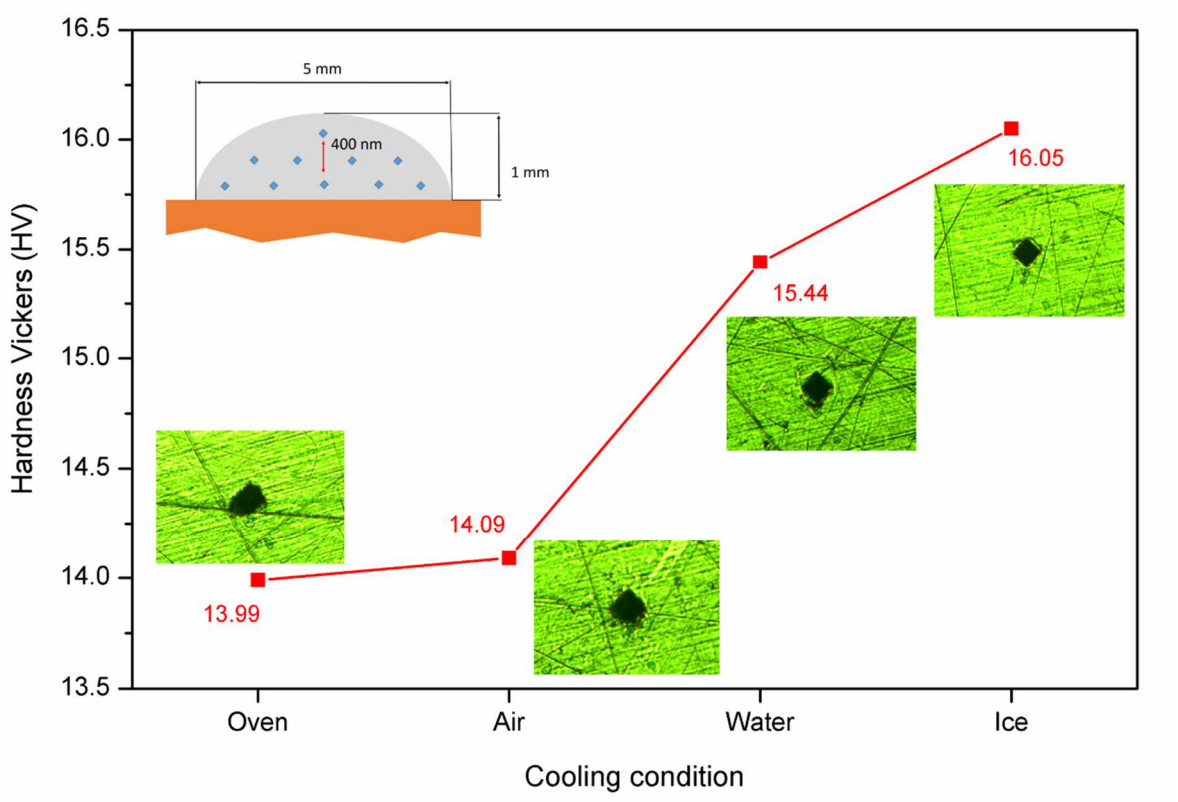

Figure 9: Schematic of IMC formation at solder/substrate interface and at bulk for: (a) oven cooled, (b) air cooled, (c) water quenched, and (d) ice quenched solder joints.

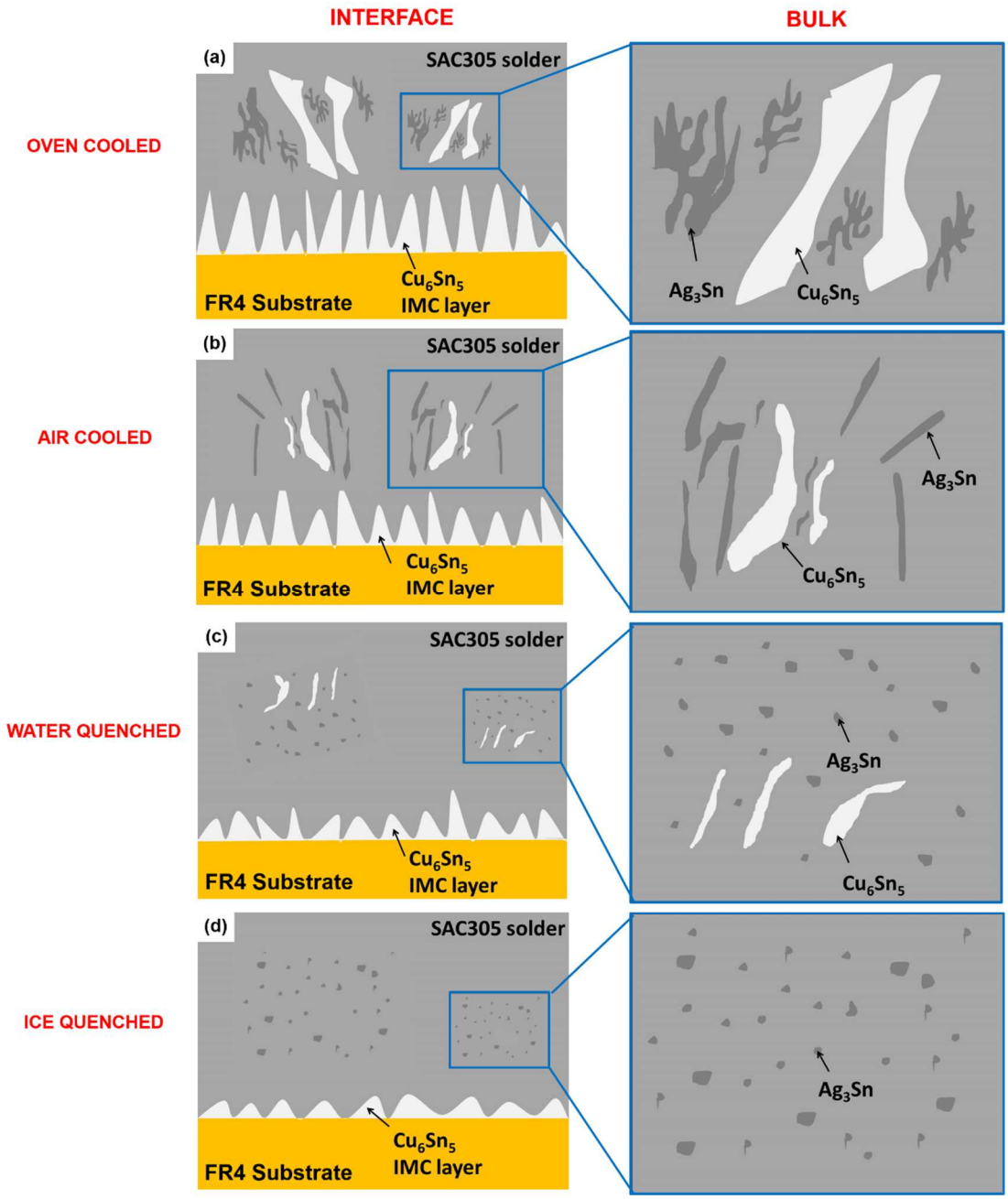

Table 1: Thickness of the Cu_6Sn_5 IMC layer of the SAC305 with different cooling conditions

Cooling condition	Cu_6Sn_5 Thickness (μm)		
	Chemical	Deep	Electrochemical
Oven cooled	4.676	3.944	3.676
Air cooled	3.849	3.501	3.411
Water quenched	2.541	2.113	1.734
Ice quenched	1.922	1.451	1.342